The Astrophysical Journal Letters, 884:L58 (7pp), 2019 October 20 https://doi.org/10.3847/2041-8213/ab48f3

First Detection of Radio Linear Polarization in a Gamma-Ray Burst Afterglow

Yuji Urata[1], Kenji Toma[2,3], Kuiyun Huang[4], Keiichi Asada[5], Hiroshi Nagai[6,7], Satoko Takahashi[7,8,9], Glen Petitpas[10], Makoto Tashiro[11], and Kazutaka Yamaoka[12,13]
[1] Institute of Astronomy, National Central University, Chung-Li 32054, Taiwan; urata@g.ncu.edu.tw
[2] Frontier Research Institute for Interdisciplinary Sciences, Tohoku University Sendai 980-8578, Japan
[3] Astronomical Institute, Tohoku University, Sendai, 980-8578, Japan
[4] Center for General Education, Chung Yuan Christian University, Taoyuan 32023, Taiwan
[5] Academia Sinica Institute of Astronomy and Astrophysics, Taipei 106, Taiwan
[6] National Astronomical Observatory of Japan, 2-21-1 Osawa, Mitaka Tokyo 181-8588, Japan
[7] Department of Astronomical Science, School of Physical Sciences, SOKENDAI (The Graduate University for Advanced Studies), Mitaka, Tokyo 181-8588, Japan
[8] Joint ALMA Observatory, Alonso de Cordova 3108, Vitacura, Santiago, Chile
[9] NAOJ Chile Observatory, Alonso de Cordova 3788, Oficina 61B, Vitacura, Santiago, Chile
[10] Harvard-Smithsonian Center for Astrophysics, 60 Garden Street, Cambridge MA 02138, USA
[11] Department of Physics, Saitama University, Shimo-Okubo, Saitama 338-8570, Japan
[12] Institute for Space-Earth Environmental Research (ISEE), Nagoya University, Furo-cho, Chikusa-ku, Nagoya, Aichi 464-8601, Japan
[13] Division of Particle and Astrophysical Science, Graduate School of Science, Nagoya University, Furo-cho, Chikusa-ku, Nagoya, Aichi 464-8601, Japan
Received 2019 April 17; revised 2019 September 27; accepted 2019 September 28; published 2019 October 21

Abstract

We report the first detection of radio polarization of a gamma-ray burst (GRB) afterglow with the first intensive combined use of telescopes in the millimeter and submillimeter ranges for GRB 171205A. The linear polarization degree in the millimeter band at the subpercent level ($0.27\% \pm 0.04\%$) is lower than those observed in late-time optical afterglows (weighted average of $\sim$1%). The Faraday depolarization by nonaccelerated, cool electrons in the shocked region is one of the possible mechanisms for the low value. This scenario requires a total energy that is larger by a factor of $\sim$10 than ordinary estimates without considering nonaccelerated electrons. The polarization position angle varies by at least 20° across the millimeter band, which is not inconsistent with this scenario. This result indicates that polarimetry in the millimeter and submillimeter ranges is a unique tool for investigating GRB energetics, and coincident observations with multiple frequencies or bands would provide more accurate measurements of the nonaccelerated electron fraction.

Key words: acceleration of particles – gamma-ray burst: individual (GRB171205A) – polarization

1. Introduction

Gamma-ray bursts (GRBs) are highly energetic explosions in the universe, and are currently being exploited as probes of first-generation stars and gravitational wave transients. In fact, the distant events at the reionization epoch (Tanvir et al. 2009; Cucchiara et al. 2011; Totani et al. 2014) and the short GRB coincident with a gravitational wave transient have already been observed (Abbott et al. 2017), respectively. The energetics of GRBs are fundamental physical parameters that can not only reveal their progenitor systems but also probe both the early and current states of the universe (e.g., Murase et al. 2006; Toma et al. 2016; Kawaguchi et al. 2018). Although substantial observational efforts have been made since the afterglow discovery (Costa et al. 1997), the total energies have been estimated so far without considering nonaccelerated, cool electrons at the relativistic collisionless shocks that do not emit observable radiation (Eichler & Waxman 2005), while the existence of such cool electrons is well studied for supernova remnants and solar winds (e.g., van Adelsberg et al. 2008; Vink et al. 2015). In GRB afterglows, the presence of nonaccelerated electrons would induce Faraday effects on the emitted radiation. Observationally, this manifests as a suppression of the radio polarization but keeps the optical polarization as emitted (Toma et al. 2008).[14] Here, we report the first detection of radio polarization of a GRB afterglow through observing low-luminosity GRB 171205A, and discuss implications for the Faraday depolarization model.

GRB 171205A was detected on 2017 December 5, 07:20:43 UT (D'Elia et al. 2017) and its X-ray and optical afterglows (D'Elia et al. 2018) are identified by the Neil Gehrels Swift Observatory. Izzo et al. (2017) made spectroscopic observations with the Very Large Telescope in Chile approximately 1.5 hr after the GRB by identifying the optical afterglow and, based on the absorption and emission lines, announced a redshift of $z = 0.0368$. At this redshift, the isotropic γ-ray energy release $E_{\gamma,\mathrm{iso}}$ of 2.4×10^{49} erg (in the 20−1500 keV range with the cosmological parameters $H_0 = 70$ km s^{-1} Mpc^{-1}, $\Omega_m = 0.3$, and $\Omega_\Lambda = 0.7$) indicates that GRB 171205A is categorized as a low-luminosity GRB. Intensive optical photometric and spectroscopic observations using the 10.4 m Gran Telescopio CANARIAS revealed the association of a broad-line type Ic supernova that resembled SN 1998bw (de Ugarte Postigo et al. 2017). The bright millimeter afterglow was also detected by the Northern Extended Millimeter Array in the 90 and 150 GHz bands 20.2 hr after the burst (de Ugarte Postigo et al. 2017).

2. Observations and Analysis

2.1. Submillimeter Array (SMA)

Intensive total flux monitoring was made using the SMA at 230 GHz starting on 2017 December 6 with a total of six epochs. On the nights of 2017 December 8 and 13, the afterglow was observed by the dual-band mode at 230 and 345 GHz. The data were flagged and calibrated with the MIR data-reduction package using standard procedures and were then imaged using Miriad software (Sault et al. 1995). Except for the observation at 345 GHz on 2017 December 13 (due to marginal weather

[14] Spectroscopic searches of nonaccelerated electrons are discussed in Ressler & Laskar (2017) and Warren et al. (2018).

Table 1
Polarization and Photometric Observing Log

Polarimetry Epoch1: 2017-Dec-10 10:23-13:17, T = 5.187 days						
SPW	Frequency (GHz)	Polarization (%)	P.A. (Degree)	I Flux (mJy)	Q Flux (mJy)	U Flux (mJy)
0,1,2,3	97.5	0.27 ± 0.04	−71.3 ± 3.3	31.944 ± 0.440	−0.069 ± 0.009	−0.053 ± 0.011
0	90.5	0.30 ± 0.06	−67.9 ± 4.7	32.719 ± 0.413	−0.070 ± 0.010	−0.069 ± 0.020
1	92.4	<0.32	<−78.1 or >78.1	32.514 ± 0.365	−0.094 ± 0.026	0.014 (rms)
2	102.5	0.35 ± 0.08	−71.3 ± 5.5	31.172 ± 0.399	−0.086 ± 0.025	−0.066 ± 0.018
3	104.5	0.31 ± 0.06	−58.0 ± 4.9	30.898 ± 0.412	−0.043 ± 0.012	−0.087 ± 0.029
Polarimetry Epoch2: 2017-Dec-16 11:14-14:33, T = 11.231 days						
SPW	Frequency (GHz)	Polarization (%)	P.A. (Degree)	I Flux (mJy)	Q Flux (mJy)	U Flux (mJy)
All	97.5	<0.27	⋯	15.705 ± 0.090	0.010 (rms)	0.010 (rms)
0	90.5	<0.52	⋯	16.171 ± 0.106	0.020 (rms)	0.020 (rms)
1	92.4	<0.52	⋯	16.054 ± 0.110	0.019 (rms)	0.019 (rms)
2	102.5	<0.52	⋯	15.370 ± 0.113	0.019 (rms)	0.019 (rms)
3	104.5	<0.54	⋯	15.206 ± 0.111	0.019 (rms)	0.019 (rms)
Total Flux Observation Log						
Instrument	Epoch (Days)	Frequency (GHz)	Flux (mJy)			
VLA	4.306	5.0	2.41 ± 0.12			
VLA	4.306	7.1	4.32 ± 0.05			
VLA	4.306	8.5	5.71 ± 0.05			
VLA	4.306	11.0	8.42 ± 0.06			
VLA	4.306	13.5	11.26 ± 0.09			
VLA	4.306	16.0	14.01 ± 0.11			
SMA	1.496	230	53.6 ± 0.9			
SMA	2.412	230	48.4 ± 0.6			
SMA	3.478	230	41.2 ± 0.8			
SMA	4.272	230	30.0 ± 0.7			
SMA	8.398	230	11.1 ± 1.0			
SMA	11.033	230	8.9 ± 0.4			
SMA	3.478	345	21.9 ± 2.3			
ACA	5.126	345	17.0 ± 0.8			
ACA	7.069	345	12.9 ± 0.1			
SMA	8.398	345	>15.8			
ACA	11.180	345	6.9 ± 0.3			

conditions in the band), the afterglow was clearly detected at a confidence level of more than 10σ. Flux measurements were performed using Common Astronomy Software Applications (CASA, version 5.1.1; McMullin et al. 2007). We measured a bright submillimeter afterglow of 53.7 ± 0.9 mJy in the 230 GHz band 1.5 days after GRB, which is the brightest afterglow ever detected in the submillimeter range. At the same epoch, the historic GRB030329 was 49.2 ± 1.1 mJy in the 250 GHz band (Sheth et al. 2003), while typical submillimeter-detected afterglows are orders of magnitude fainter (Urata et al. 2014, 2015). Thus, GRB 171205A is an ideal object for performing the first radio polarimetry.

2.2. The Atacama Large Millimeter/submillimeter Array (ALMA)

ALMA observed the afterglow in two different epochs using the linear polarization mode at Band 3 (representative frequency of 97.5 GHz) on 2017 December 10 and 16. The correlator processed four spectral windows (SPWs) centered at 90.5, 92.5, 102.5, and 104.5 GHz with a bandwidth of 1.75 GHz each. The bandpass and flux were calibrated using observations of J1127–1857, and J1130–1149 was used for the phase calibration. The polarization calibration was performed by observations of J1256-0547. The raw data were reduced at the East Asian ALMA Regional Center (EA-ARC) using CASA (version 5.1.1). We further performed interactive CLEAN deconvolution imaging with self-calibration of both amplitude and phase with infinite and then 30 s solution intervals. The Stokes I, Q, and U maps were CLEANed up to 15,000 of CLEAN iterations with a threshold of 0.02 mJy after the final round of self-calibration (Figure 1(a)). The off-source rms levels in I, Q, and U are consistent with the expectations for thermal noise alone. Since the detections with high signal-to-noise ratio were made on the Stokes Q and U maps generated using the entire Band 3 data set from 2017 December 10, we generated additional Stokes maps using the individual SPWs (Figures 1(b)–(e)). The quantities that can be derived from the polarization maps are the polarized intensity ($\sqrt{Q^2+U^2}$), polarization degree ($100\ \sqrt{Q^2+U^2}/I\%$), and polarization position angle ($1/2\arctan(U/Q)$, P.A.). The *atan*2 function in the python math module which returns a numeric value between $-\pi$ and π, was used to calculate the polarization position angle. By applying the polarization calibration to the phase calibrator J1130–1449 and creating Stokes maps for 6, 9, and 18 epochs during the 3 hr observing period, we confirm that the stability of linear polarization degree is <0.02%, which is consistent with the systematic linear polarization calibration uncertainty of 0.033%

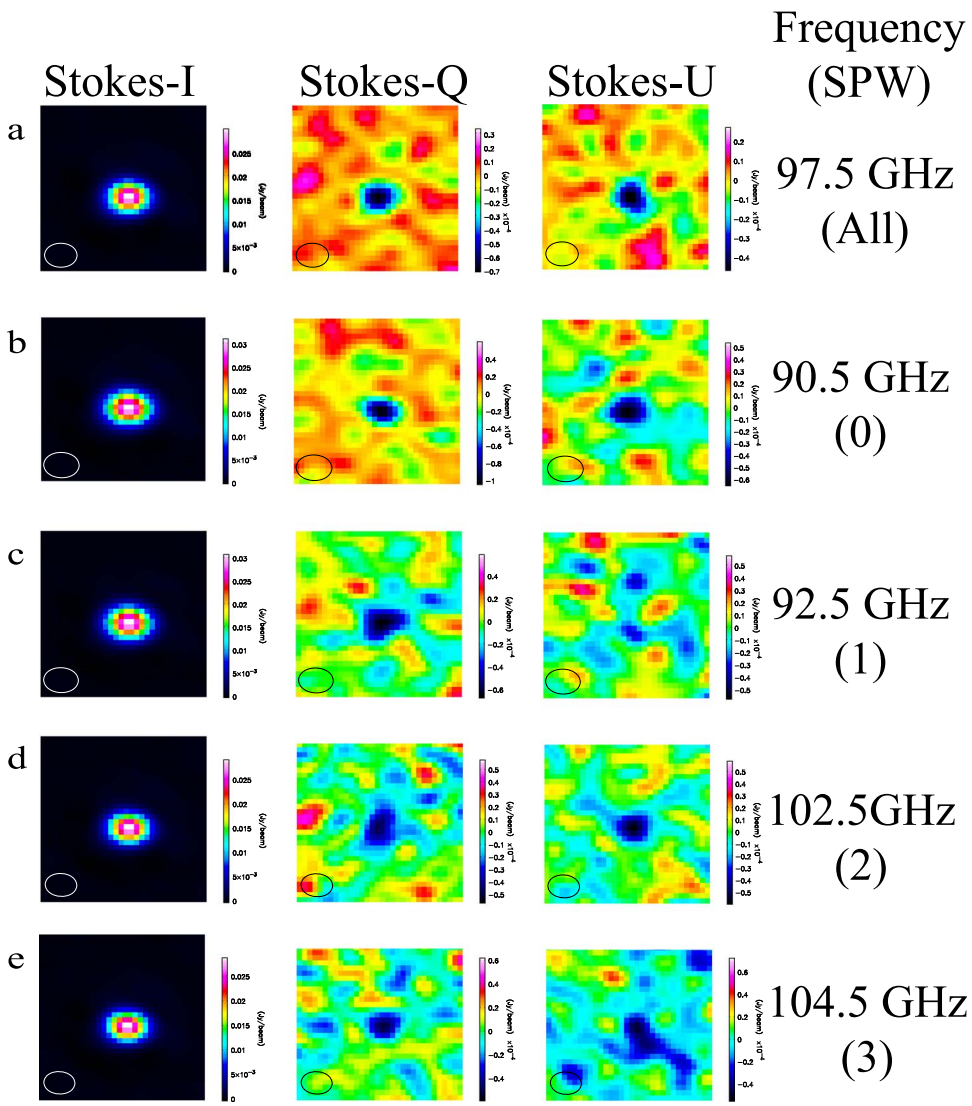

Figure 1. Stokes *I*, *Q*, and *U* maps ($5'' \times 3''$) of the afterglow of GRB 171205A taken on 2018 December 10 (5.187 days after the burst). The ALMA beam size is shown with the open cyan circles. The map created using the entire ALMA Band 3 data set with a representative frequency of 97.5 GHz (a), and four individual spectral windows (SPW) with a representative frequency of 90.5 GHz (b), 92.5 GHz (c), 102.5 GHz (d), and 104.5 GHz (e). The units of color bars are mJy for Stokes *I* and μJy for Stokes *Q* and *U* maps.

for compact sources.[15] We also find that the stability of P.A. is $<0.^{\circ}6$, which is slightly larger than the absolute accuracy of $0.^{\circ}3$ (Nagai et al. 2016). The nondetection (both positive and negative) with a signal-to-noise ratio (S/N) of 3 on the 92.5–GHz *U* map taken on 2017 December 10 yielded polarization position angle ranges of P.A. $> +78^{\circ}$ and P.A. $< -78^{\circ}$.

The Atacama Compact Array (ACA) observations were executed on 2017 December 10, 12, and 16 at 345 GHz (Band 7) with the single continuum observing mode. Two of the ACA total flux measurements were conducted during polarimetry using ALMA. The data were flagged, calibrated, and imaged with standard procedures with CASA (version 5.1.1).

2.3. Very Large Array (VLA)

The VLA made total flux measurements for the afterglow on 2017 December 9 at central frequencies of 6 GHz (*C*-band), 10 GHz (*X*-band), and 15 GHz (*U*-band), as one of the observatory-sponsored observations (Laskar et al. 2017). The phase and flux were calibrated using observations of J1130-1449 and 3C286. The data were calibrated using standard tools in CASA (VLA pipeline version 5.0.0). After checking the quality of the pipeline output, we performed imaging using the CLEAN task without additional data flagging. The source was significantly (more than 50σ) detected in all three bands. To describe the spectral energy distribution, six images at the central frequencies of 5, 7, 8.5, 11, 13.5, and 16 GHz were generated with the CLEAN task. The afterglow was detected with $>20\sigma$ significance in each image and the resulting total flux densities are summarized in Table 1.

3. Results

3.1. Light Curve and Spectral Energy Distribution

The temporal evolution of the afterglow flux at 230 GHz is described by broken power-law decays ($F_\nu \propto t^\alpha$) with $\alpha = -0.30 \pm 0.07$ for $t \lesssim 4$ days and $\alpha = -1.34 \pm 0.06$ for $t \gtrsim 4$ days, as shown in Figure 2. The light curve at

[15] ALMA technical handbook; https://almascience.nrao.edu/documents-and-tools/cycle7/alma-technical-handbook/.

345 GHz for $t \gtrsim 4$ is also described by a simple power-law with $\alpha = -1.2 \pm 0.2$. The spectral slope ($F_\nu \propto \nu^\beta$) is also described as $\beta = 1.457 \pm 0.028$ at 4.3 days in the centimeter range (5–16 GHz; Figure 3(a)) and $\beta = -0.430 \pm 0.004$ at 5.2 days in the submillimeter and millimeter range (90.5–345 GHz; Figure 3(a)). High-quality photometry ($S/N \sim 72$–89) using ALMA during the polarimetry, at 5.2 days, measured the spectral slope of $\beta = -0.40 \pm 0.01$ in the 90–100 GHz (i.e., Band 3). These measurements indicate that the spectral peak was located at ∼30 GHz (below ∼90 GHz).

3.2. Polarization

Figure 1(a) shows the Stokes I, Q, and U maps obtained using the entire ALMA Band 3 frequency range taken 5.2 days after the GRB. Detections with a confidence level of 5σ or better on the Q and U maps yield a polarization degree of $0.27\% \pm 0.04\%$ (including systematic error). Our measured value describes the intrinsic origin because depolarization between the source and observing site is negligible for the point source (i.e., GRB afterglows) in this millimeter band (Brentjens & de Bruyn 2005). Although we could not find any detection in the Stokes Q and U maps at 11.2 days, we measured the corresponding deep upper limit of the polarization degree (<0.27%, 3σ significance), which was consistent with that at 5.2 days within the error margin.

The apparent brightness of 31.94 ± 0.44 mJy observed 5.2 days after the burst using the entire ALMA Band 3 frequency range enabled more detailed polarimetric analysis using four individual SPW of Band 3 (Figures 1(b)–(e)). The measurements are summarized in Table 1. Other than the Stokes U map at 92.5 GHz, there were significant detections at a 3.0σ confidence level or better. In the Stokes U map at 92.5 GHz, there was no significant flux, and the range of the P.A. was constrained. Although the polarization degrees in each SPW were consistent with the value measured using the entire Band 3 frequency, the P.A. significantly varied with the wavelength (Figure 4). The observed P.A. is most likely an intrinsic value because the Faraday rotation effect for both the host galaxy and the Milky Way is quite small at this frequency (Sokoloff et al. 1998; Oppermann et al. 2012). The expected galactic Faraday rotation effect is up to ∼0°.3. We tried to fit the P.A. data including the upper limit (the method is described in Sawicki 2012) with a constant or linear function of squared wavelength, but did not obtain a good fit (Figure 4).

4. Discussion

4.1. Afterglow Modeling

We find that the spectra of Figure 3(a) can be well fitted by the forward shock synchrotron emission model by Granot & Sari (2002) with the synchrotron self-absorption frequency $\nu_a \sim 20$ GHz and the synchrotron frequency of minimum-energy electrons $\nu_m \sim 200$ GHz. In such a late phase the slow cooling regime (i.e., $\nu_m < \nu_c$) is likely. Then the observed shallow decay at $t \lesssim 4$ days may correspond to the spectral segment $\nu_a < \nu < \nu_m$. If the spectrum in this segment is the power-law with $\beta = 1/3$, the decay index is $\alpha = 3\beta/2 - 1/2 = 0$ in the wind environment case (Zhang & Mészáros 2004). However, our smoothly broken power-law spectrum ($\beta < 1/3$ effectively, see Figure 3(a)) leads to a steeper decay, which cannot fit the observed 230 GHz light curve at $t \lesssim 4$ days.

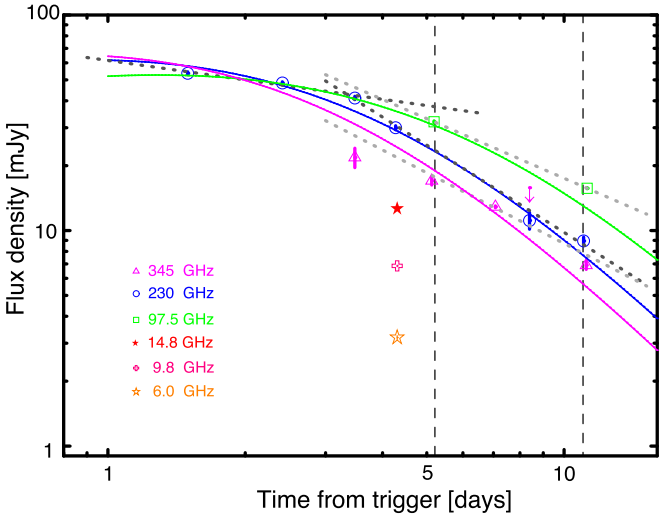

Figure 2. Radio afterglow light curves. Solid lines indicate the model light curves at 97.5 (green), 230 (blue), and 345 GHz (magenta) based on the standard forward shock model. Dark gray dotted lines show the simple power-law fittings for 230 GHz data before and 4 days after the burst. Light gray dotted lines show the simple power-law functions for 97.5 GHz with $\alpha = -0.9$ and 345 GHz with $\alpha = -1.2$. Thin black dashed lines indicate the epochs of ALMA polarimetry.

Alternatively, we find that the interstellar matter (ISM) environment case can fit it well.

The flux after ν_m crosses the observed frequency (i.e., $\nu_m < \nu < \nu_c$) obeys the closure relation $\alpha - 3\beta/2 = 0$ (Zhang & Mészáros 2004) in the ISM environment case when the edge of the collimated shock is not observed. After the edge is observed (but the shock does not expand sideways; Zhang & MacFadyen 2009), the additional geometrical flux reduction $\Gamma^2\theta_j^2 \propto t^{-3/4}$ leads to $\alpha - 3\beta/2 = -3/4$, where Γ and θ_j are the Lorentz factor and opening half-angle of the shock, respectively. The latter relation is consistent with the observed relation $\alpha - 3\beta/2 \simeq -0.69 \pm 0.07$.

Based on the above consideration, we adopt the flux formula of Granot & Sari (2002) multiplied by the geometrical flux reduction factor $[1 + (t/t_j)]^{-3/4}$ to fit the observed data (Figures 2, 3(a)). Here we set the synchrotron self-absorption frequency $\nu_a \simeq 22$ GHz, the synchrotron frequency of minimum-energy electrons $\nu_m \simeq 200\,(t/4.3\ \mathrm{days})^{-3/2}$ GHz, the peak flux before the jet break $F_{\nu m}$ ($t < t_j$) $\simeq 72$ mJy, the jet break time $t_j \simeq 2$ days, and the electron energy spectral index $p \simeq 3$. The first three characteristic quantities are functions of four physical parameters, namely the isotropic shock energy $E_{\rm iso}$, the ambient medium density n, the fraction of shock energy carried by the electrons ϵ_e, and that carried by amplified magnetic field ϵ_B. Thus, we have the relations $n \simeq 600\,(E_{\rm iso}/5 \times 10^{48}\ \mathrm{erg})^3\ \mathrm{cm}^{-3}$, $\epsilon_e \simeq 0.3\,(E_{\rm iso}/5 \times 10^{48}\ \mathrm{erg})$, and $\epsilon_B \simeq 0.2\,(E_{\rm iso}/5 \times 10^{48}\ \mathrm{erg})^{-5}$. The numerical values of n, ϵ_e, and ϵ_B are not unrealistic (Panaitescu & Kumar 2002), and $E_{\rm iso}$ should not be considerably different from this value because of $\epsilon_e < 1$ and $\epsilon_B < 1$. For these values we calculated the X-ray light curve, which does not overwhelm the observed one. This analysis means that we found a possible physical afterglow model (while we leave a full exploration of possible models for a separate work), and supports our argument that we performed the first radio afterglow polarimetry in the waveband well above ν_a (see Granot & Taylor 2005; van der Horst et al. 2014).

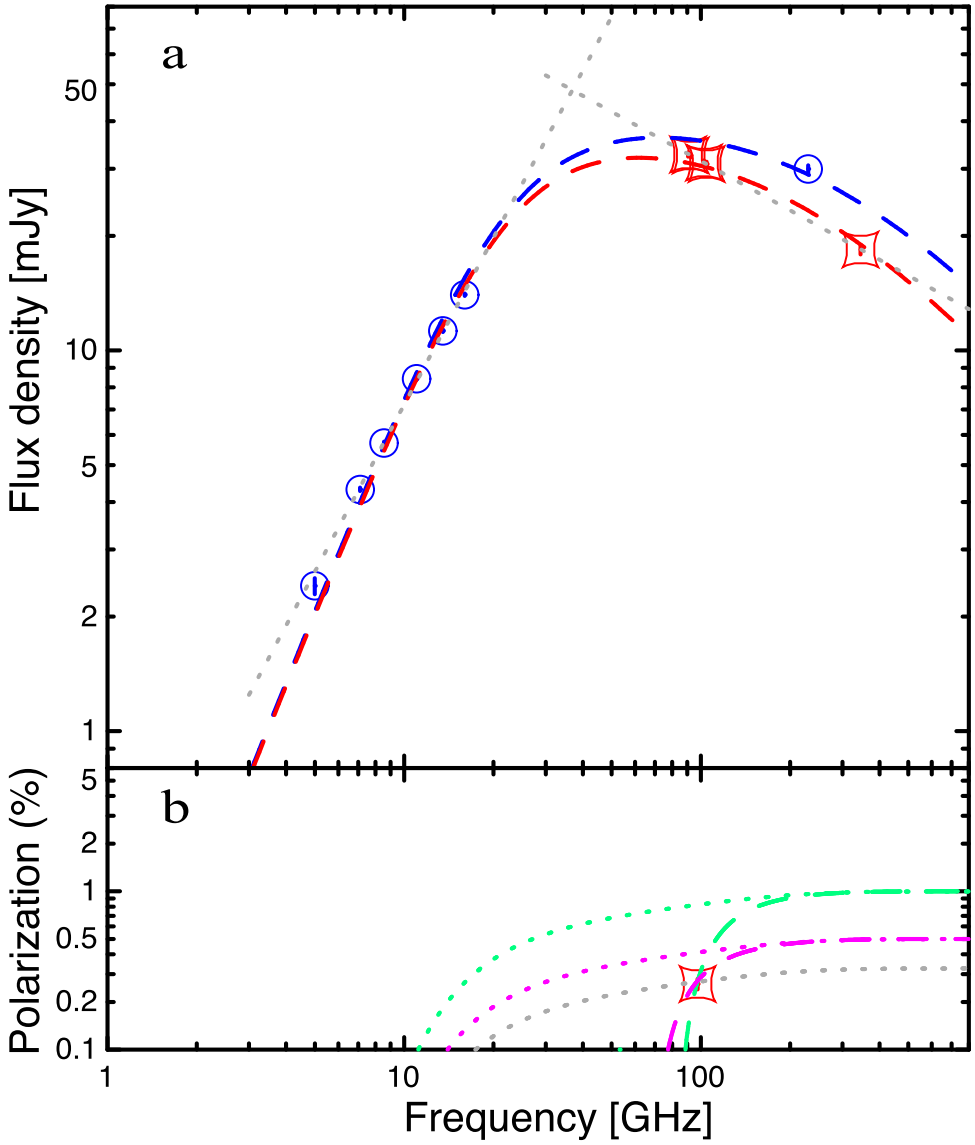

Figure 3. Spectral flux distributions and total linear polarization spectrum of the GRB 171205A afterglow. (a) Spectral flux distribution at 4.1 days (blue circles and model dashed line) and 5.2 days (red squared points and model dashed line) after burst. The gray dotted lines indicate the simple power-law functions with indexes of 1.457 and −0.430. (b) Total linear polarization spectrum with the ALMA measurement 5.2 days after the burst. Dashed lines indicate the Faraday depolarized spectrum by assuming P_0 of 1% (green) and 0.5% (magenta). The dotted lines indicate the polarization spectrum without the Faraday depolarization effect (i.e., all electrons are energized by the relativistic shock) by assuming P_0 of 1% (green), 0.5% (magenta), and 0.33% (gray).

4.2. Faraday Depolarization Effect

We focused on the polarization at 5.2 days, the phase when the intensity can be explained by the standard forward shock model. The precise detection of the polarization degree of $0.27\% \pm 0.04\%$ indicated that the value is the smallest one among all afterglow polarization measurements, and smaller than those in late-time optical afterglows explained by the standard forward shock model, which range from 0.5% to 10% (Greiner et al. 2003; Wiersema et al. 2014; Covino & Gotz 2016).[16]

There was no polarimetric data at the higher frequency ranges for the present event (except the supernova component in the optical band). Note that there are 84 polarimetric measurements for optical afterglows (i.e., excluding measurements for early-time reverse shock components that show high values) among 13 GRBs (Covino & Gotz 2016). The weighted average and average of the measurements are 1.0% and 1.6%, respectively. Among these, 58 measurements were made during the phases in which the intensities are describable by the standard forward shock model. For these selected events, the weighted average and average of the linear polarizations are 1.2% and 1.7%, respectively.

By assuming a polarization degree at higher frequency ranges (e.g., optical) for the present event as $P_0 = 1\%$, we calculate the polarization spectrum based on the afterglow model described above (see Jones & O'Dell 1977; Matsumiya & Ioka 2003; Sagiv et al. 2004; Huang & Shcherbakov 2011), and plot it by the green dotted line in Figure 3(b). It varies by a factor of $0.5(p + 7/3)/(p + 1) \simeq 2/3$ at $\nu = \nu_m$ and decays at $\nu \lesssim \nu_a$. Our measured value is substantially lower than this model line.

[16] Although the minimum value of 0.31% was measured with the GRB 030329 optical afterglow, the measurement was performed during the multiple bump light-curve phase with strong polarization variabilities (i.e., extra physical explanations to the standard afterglow model are required).

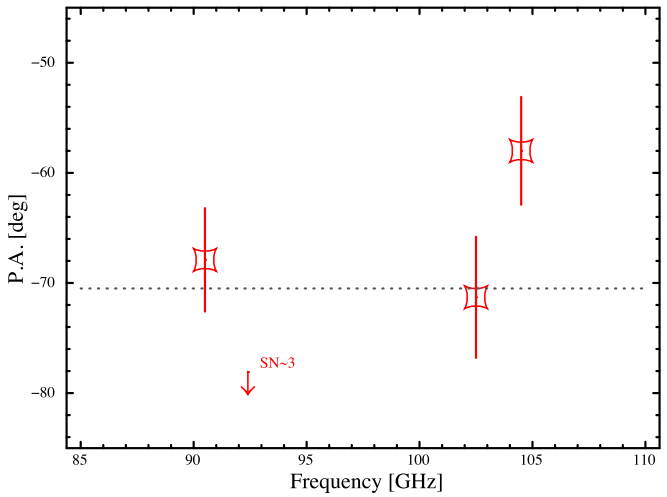

Figure 4. Position angle (P.A.) of the GRB 171205A afterglow as a function of wavelength. Squared points indicate the observed P.A. at 90.5, 102.5, and 104.5 GHz. The upper limit at 92.5 GHz with a signal-to-noise ratio of 3 is also plotted with a red arrow. The gray dotted line indicates the constant fitting function with a reduced chi-square of 4.5 (d.o.f = 3).

If only part of the swept-up electrons is accelerated, the nonaccelerated electrons with thermal Lorentz factor $\tilde{\gamma}_m = \eta\Gamma$ cause Faraday depolarization at $\nu > \nu_a$ (Toma et al. 2008), where η is a factor of the order of unity in the case that the nonaccelerated electrons are just isotropized at the shock front (Eichler & Waxman 2005). Such a model in which the fraction of accelerated electrons is $f < 1$ can explain the intensity in the same way as in the standard model with the parameters $E_{\rm iso}{}' = E_{\rm iso}/f$, $n' = n/f$, $\epsilon_e' = \epsilon_e f$, and $\epsilon_B' = \epsilon_B f$ (Eichler & Waxman 2005). Thus, a very small value of f would lead to a crisis of the total energy requirement. In this scenario, the polarization degree is given by $P_0 \sin(\tilde{\gamma}_V/2)/(\tilde{\gamma}_V/2)$ where $\tilde{\gamma}_V = (\nu/\tilde{\nu}_V)^{-2}$ and $\tilde{\nu}_V \sim 200\,[(1-f)/10f]^{1/2}\eta^{-1}\sqrt{\ln\tilde{\gamma}_m}N^{-1/12}(E_{\rm iso}/10^{52}\ {\rm erg})^{3/16}$ $n^{9/16}(\epsilon_B/0.01)^{1/4}(t/1\ {\rm day})^{-1/16}$ GHz. Here the magnetic field in the shocked region has been assumed to be tangled on hydrodynamic scales, following Toma et al. (2008) and Uehara et al. (2012), and the plasma can be considered to consist of a number of random cells, in each of which magnetic field is ordered (Jones & O'Dell 1977; Gruzinov & Waxman 1999). N denotes the number of random cells in the three-dimensional visible region. In this case $P_0 = (p+1)/[(p+7/3)\sqrt{N}]$ for $\nu > \nu_m$ while $P_0 = 0.5/\sqrt{N}$ for $\nu_a < \nu < \nu_m$. With $P_0 = 1\%$ for $\nu > \nu_m$, $\tilde{\nu}_V \simeq 210$ GHz explains our measurement (see the green dashed line in Figure 3(b)), which corresponds to $1/f \sim 12\,(E_{\rm iso}/2\times10^{50}{\rm erg})^{-5/4}\eta^2(\ln\tilde{\gamma}_m)^{-1}$. For the case of $P_0 = 0.5\%$ (Figure 3(b)), $1/f \sim 10$ is still required. For the case of $P_0 = 10\%$, $1/f \sim 60$ is required. We should also note that the case of $P_0 \simeq 0.33\%$ is not ruled out (see Figure 3(b)), where the Faraday depolarization effect with $f < 1$ is not required.

The P.A. becomes a very complicated function of wavelength and the functional form is determined randomly for a tangled magnetic field such as the one we assume (Sokoloff et al. 1998). Therefore, the observed variation of the P.A. is not inconsistent with this scenario.

In summary, with the first intensive combined use of telescopes in the millimeter and submillimeter ranges for the GRB 171205A afterglow, our observations provided the first linear polarimetry in the millimeter band. The measured polarization degree is substantially lower than the typical optical one. Although the (semi)simultaneous measurements in multiple wavelengths are required, this measurement suggests the Faraday depolarization effect and a total energy that is a factor of ∼10 larger than the ordinary estimate without considering nonaccelerated electrons. The observed P.A. variation along with wavelength is not inconsistent with this scenario. Multifrequency polarimetry in the submillimeter/millimeter range and/or with simultaneous optical polarimetry would provide a more accurate nonaccelerated electron fraction. Hence, this observation consolidates the new methodology for revealing the fundamental properties of GRBs.

We thank the anonymous referee for a careful review of our manuscript. This paper makes use of the following ALMA data: ADS/JAO.ALMA#2017.1.00801.T. ALMA is a partnership of ESO (representing its member states), NSF (USA), and NINS (Japan), together with NRC (Canada), *MOST* and ASIAA (Taiwan), and KASI (Republic of Korea), in cooperation with the Republic of Chile. The Joint ALMA Observatory is operated by ESO, AUI/NRAO, and NAOJ. This work is supported by the Ministry of Science and Technology of Taiwan grants MOST 105-2112-M-008-013-MY3 (Y.U.) and 106-2119-M-001-027 (K.A.). This work is also supported by JSPS Grants-in-Aid for Scientific Research No. 18H01245 (K.T.). We thank EA-ARC, especially Pei-Ying Hsieh for support in the ALMA observations. We also thank P. T. P. Ho and Y. Ohira for helpful comments. Y.U, K.Y.H., and K.A. also thank the Ministry of Education Republic of China.

Facilities: ALMA, SMA, VLA.

Software: CASA (McMullin et al. 2007).

ORCID iDs

Yuji Urata https://orcid.org/0000-0001-7082-6009
Kenji Toma https://orcid.org/0000-0002-7114-6010
Hiroshi Nagai https://orcid.org/0000-0003-0292-3645
Satoko Takahashi https://orcid.org/0000-0002-7287-4343

References

Abbott, B. P., Abbott, R., Abbott, T. D., et al. 2017, ApJL, 848, L13
Brentjens, M. A., & de Bruyn, A. G. 2005, A&A, 441, 1217
Costa, E., Frontera, F., Heise, J., et al. 1997, Natur, 387, 783
Covino, S., & Gotz, D. 2016, A&AT, 29, 205
Cucchiara, A., Levan, A. J., Fox, D. B., et al. 2011, ApJ, 736, 7
de Ugarte Postigo, A., Izzo, L., Kann, D. A., et al. 2017, GCN, 22204, 1
de Ugarte Postigo, A., Schulze, S., Bremer, M., et al. 2017, GCN, 22187, 1
D'Elia, V., Campana, S., D'Aì, A., et al. 2018, A&A, 619, A66
D'Elia, V., D'Ai, A., Lien, A. Y., & Sbarufatti, B. 2017, GCN, 22177, 1
Eichler, D., & Waxman, E. 2005, ApJ, 627, 861
Granot, J., & Sari, R. 2002, ApJ, 568, 820
Granot, J., & Taylor, G. B. 2005, ApJ, 625, 263
Greiner, J., Klose, S., Reinsch, K., et al. 2003, Natur, 426, 157
Gruzinov, A., & Waxman, E. 1999, ApJ, 511, 852
Huang, L., & Shcherbakov, R. V. 2011, MNRAS, 416, 2574
Izzo, L., Selsing, J., Japelj, J., et al. 2017, GCN, 22180, 1
Jones, T. W., & O'Dell, S. L. 1977, ApJ, 214, 522
Kawaguchi, K., Shibata, M., & Tanaka, M. 2018, ApJL, 865, L21
Laskar, T., Coppejans, D. L., Margutti, R., & Alexander, K. D. 2017, GCN, 22216, 1
Matsumiya, M., & Ioka, K. 2003, ApJL, 595, L25
McMullin, J. P., Waters, B., Schiebel, D., Young, W., & Golap, K. 2007, adass XVI, 376, 127
Murase, K., Ioka, K., Nagataki, S., et al. 2006, ApJL, 651, L5
Nagai, H., Nakanishi, K., Paladino, R., et al. 2016, ApJ, 824, 132
Oppermann, N., Junklewitz, H., Robbers, G., et al. 2012, A&A, 542, A93
Panaitescu, A., & Kumar, P. 2002, ApJ, 571, 779
Ressler, S. M., & Laskar, T. 2017, ApJ, 845, 150

Sagiv, A., Waxman, E., & Loeb, A. 2004, ApJ, 615, 366
Sault, R. J., Teuben, P. J., & Wright, M. C. H. 1995, adass IV, 77, 433
Sawicki, M. 2012, PASP, 124, 1208
Sheth, K., Frail, D. A., White, S., et al. 2003, ApJL, 595, L33
Sokoloff, D. D., Bykov, A. A., Shukurov, A., et al. 1998, MNRAS, 299, 189
Tanvir, N. R., Fox, D. B., Levan, A. J., et al. 2009, Natur, 461, 1254
Toma, K., Ioka, K., & Nakamura, T. 2008, ApJL, 673, L123
Toma, K., Yoon, S.-C., & Bromm, V. 2016, SSRv, 202, 159
Totani, T., Aoki, K., Hattori, T., et al. 2014, PASJ, 66, 63
Uehara, T., et al. 2012, ApJL, 752, L6
Urata, Y., Huang, K., Asada, K., et al. 2015, AdAst, 2015, 165030
Urata, Y., Huang, K., Takahashi, S., et al. 2014, ApJ, 789, 146
van Adelsberg, M., Heng, K., McCray, R., & Raymond, J. C. 2008, ApJ, 689, 1089
van der Horst, A. J., Paragi, Z., de Bruyn, A. G., et al. 2014, MNRAS, 444, 3151
Vink, J., Broersen, S., Bykov, A., & Gabici, S. 2015, A&A, 579, A13
Warren, D. C., Barkov, M. V., Ito, H., Nagataki, S., & Laskar, T. 2018, MNRAS, 480, 4060
Wiersema, K., Covino, S., Toma, K., et al. 2014, Natur, 509, 201
Zhang, B., & Mészáros, P. 2004, IJMPA, 19, 2385
Zhang, W., & MacFadyen, A. 2009, ApJ, 698, 1261